RSC Advances

COMMUNICATION

View Article Online
View Journal | View Issue

Cite this: *RSC Adv.*, 2016, **6**, 27677

Received 21st January 2016
Accepted 3rd March 2016

DOI: 10.1039/c6ra01836j

www.rsc.org/advances

Photoinduced doping and photoluminescence signature in an exfoliated WS_2 monolayer semiconductor

X. H. Wang,†[abc] J. Q. Ning,†[abcd] Z. C. Su,[abc] C. C. Zheng,[abce] B. R. Zhu,[a] L. Xie,[a] H. S. Wu[a] and S. J. Xu*[abc]

Following graphene, atomically thin two-dimensional transition metal dichalcogenides (2D-TMDs) are quickly emerging as a new multidisciplinary frontier across condensed matter physics, materials science and inorganic chemistry. Compared with graphene, the optical and optoelectronic properties of 2D-TMD materials are more attractive largely due to the nature of their direct band gap. In this article, we show an interesting demonstration of the photoinduced doping effect in a mechanically-exfoliated high-quality tungsten disulfide (WS_2) monolayer semiconductor. By utilizing a focused laser beam and increasing its intensity, we successfully observed a photoinduced doping effect, indicated by the gradual tuning of dominant light emission from a single narrow emission band peaking at 2.017 eV (Peak 1) to a broad asymmetric emission band (Peak 2) eventually located at around 1.955 eV at room temperature. Moreover, the peak position of Peak 2 shows a distinct red shift dependence on the excitation intensity, predicted by the band gap renormalization theory due to the heavy doping. Justified from their spectral features and excitation intensity dependence, the narrow emission band is ascribed to the fundamental band edge free exciton transition, whereas the broad asymmetric one is ascribed to the localized state ensemble induced by photo doping.

Introduction

Atomically thin monolayers of transition metal dichalcogenides (TMDs) represent a new type of two-dimensional (2D) material and have attracted rapidly increasing interest since they are an analogue of graphene in a lattice structure and have application potential in nanoelectronics and optoelectronics.[1] Unlike graphene, the energy band structures of TMD monolayers show a direct band gap configuration, which has been verified both theoretically and experimentally.[2,3] This makes TMD monolayers more suitable for new nanophotonic and optoelectronic applications. It is well known that the great success of modern semiconductor technologies is based on the remarkable capability of controllable doping in fabrication processes. It should be also true for the case of TMD monolayers. In other words, the applications of TMD crystals and even graphene in the above-mentioned devices also rely on controlling dopants and defects in these two extreme two-dimensional materials.[4,5] Very recently, Kang *et al.* observed photoluminescence (PL) quenching in single-layer MoS_2 by creating defects *via* oxygen plasma treatment.[6] And by combining this with theoretical calculations, they show that the creation of MoO_3 disordered domains upon exposure to oxygen plasma leads to the observed PL quenching. We also observed that the PL intensity of CVD-grown WS_2 monolayers significantly attenuates upon continuous exposure to the focused CW laser beam (514.5 nm) due to the mass creation of atomic defects.[7] Interestingly, Chow *et al.* reported a distinct defect-related PL spectral feature located at ~0.1 eV below the neutral free A-exciton peak in WS_2 and MoS_2 monolayers.[8] They also employed plasma treatments to intentionally create atomic-scale defects in the hexagonal lattice of pristine WS_2 and MoS_2 monolayers and studied the evolution of their Raman and PL spectra.[8] In addition to the defect-related PL peak, they demonstrate that the Raman spectra of the samples treated by plasma are insensitive to defects. Hong *et al.* presented a comprehensive joint experiment theory investigation of point defects in monolayer MoS_2 prepared by different approaches.[9] They found that the dominant category of defects changes from S vacancies to Mo anti-sites depending on the sample preparation techniques and conditions. In a theoretical aspect, Erementchouk *et al.* computed electronic states bound to several types of vacancy defects in monolayer MoS_2, and

[a]*Department of Physics, The University of Hong Kong, Pokfulam Road, Hong Kong, China. E-mail: sjxu@hku.hk*

[b]*HKU-Shenzhen Institute of Research and Innovation (HKU-SIRI), The University of Hong Kong, Pokfulam Road, Hong Kong, China*

[c]*HKU-CAS Joint Laboratory on New Materials, The University of Hong Kong, Pokfulam Road, Hong Kong, China*

[d]*Suzhou Institute of Nano-tech and Nano-bionics, Chinese Academy of Sciences, Suzhou 215123, China*

[e]*Mathematics and Physics Centre, Department of Mathematical Sciences, Xi'an Jiaotong-Liverpool University, Suzhou 215123, China*

† These authors contributed equally to this work.

obtained the optical signature of those defect-related bound states.[10] These studies and findings show that controllable defect creation in 2D-TMD materials could enable tailoring of the optical properties of these materials and boost their opto-electronic device applications. In fact, several groups have demonstrated several TMD monolayer-based prototype devices including p–n junction photodiodes,[11] light-emitting diodes,[12,13] and transistors with the so-called valley Hall effect.[14]

In this work, we experimentally demonstrate a photoinduced doping effect in WS_2 monolayers exfoliated mechanically from a high-quality bulk crystal. At a low optical injection level, the WS_2 monolayers show a narrow and symmetric single luminescence band peaking at 2.017 eV at room temperature. As the optical injection level increases, a new emission band appears at the lower energy side of the 2.017 eV band, and gradually becomes the dominant structure in the PL spectrum accompanied by a substantial red shift of ~62 meV in its peak position. Spectral analysis suggests that it originates from radiative recombination of the localized state ensemble. The substantial red shift of the luminescence band is due to the band gap narrowing effect induced by photoinduced heavy doing.

Experimental

The monolayer WS_2 samples investigated in this study were prepared using two different approaches. In the first approach, the WS_2 flakes were mechanically exfoliated from a CVD-synthesized bulk crystal with Scotch tape, and then transferred onto silicon substrates with a 300 nm thick SiO_2 layer on top. The monolayer flake was then picked out from an optical microscope by means of color interference and is further confirmed by Raman spectroscopy.[7] In the second method, the monolayer WS_2 triangles were directly grown on a silicon substrate in a hot-wall furnace using high-purity WO_3 and sulfite powder as the starting materials.[7] The morphology of the samples was carefully inspected by field-emission scanning electron microscopy (SEM, Hitachi S-4800) under the conditions of low voltage and low electron beam intensity. And then they were optically characterized in detail on a WITec scanning confocal microscopy system integrated with a monochromator + CCD detector for Raman and PL spectroscopy and imaging. A 514.5 nm argon ion laser (Melles Griot) was used as the excitation source throughout this study. And it was guided with a fiber into a microcopy and focused by a 60× Nikon objective before impinging the sample. The maximum power was measured to be around 2.2 mW at the sample stage. High-resolution transmission electron microscopic images and selected area electron diffraction were measured on FEI Tecnai G2 20 S-TWIN TEM (FEI, USA).

Results and discussion

Fig. 1(a) and (b) show an optical and scanning electron microscopy (SEM) image of a mechanically-exfoliated WS_2 sample, respectively. As seen in the images, single layers can be distinguished from multiple layers due to their different contrasts. The laser exposure spots after the excitation power-dependent PL measurements were even resolved in the SEM image due to a somewhat bright contrast compared with the surrounding region. As the control samples, the furnace-grown monolayer WS_2 triangles were also measured. Fig. 1(d) depicts a high-resolution transmission electron micrograph of one triangle sample, while Fig. 1(c) illustrates the selected area electron diffraction (SAED) patterns of this sample. The SAED patterns clearly indicate the honeycomb hexagonal lattice structure of the sample. As a reference, Fig. 2(a) and (b) depict an optical and SEM image of a furnace-grown triangle WS_2 monolayer sample. Due to the contrast being too strong, only a bright red spot was seen in the optical image, showing red color luminescence from a micro-scale region on the triangle WS_2 monolayer illuminated by a focused 514.5 nm laser beam. From Fig. 2(b), we can see that the furnace-grown triangle sample has an edge length of ~2 μm.

Fig. 3 depicts the room temperature micro-PL spectra of the three WS_2 monolayer samples (T_1, F_1 and F_2) under the conditions of extremely low excitation level (~8 μW). This excitation level was two orders of magnitude lower than the usual excitation level (~2.0 mW) used in our confocal microscopy for PL and Raman measurements.[7] Clearly, very different spectral features are observed for the different samples although their PL spectra were measured at almost identical conditions. In the PL spectrum of the furnace-grown sample (*i.e.*, T_1) with a high density of defects the dominant emission band located at ~1.955 eV (marked as Peak 2) has a full width at half maximum (FWHM) of 58 meV and an asymmetric line shape, which is in good agreement with previous reports on WS_2 monolayers.[15,16] However, the PL spectra of the exfoliated monolayer flakes exhibit a much narrower peak located at 2.017 eV (denoted as Peak 1) with a highly symmetric Lorentzian line shape. In particular, only Peak 1 was observed in sample F_2. For sample F_1, double structures containing Peak 1 were resolved, as shown in Fig. 3(b). The double structure emission and sample-dependent spectral features suggest that two types of luminescence mechanisms could exist in WS_2 monolayers. It is interesting and hence of scientific significance to elucidate the luminescence mechanisms in monolayer TMD semiconductors. Sample F_2 offered a chance to address this issue because its PL spectral features show a distinctive dependence on the excitation level as shown below.

Interestingly, the light emission of sample F_2 exhibits remarkable variation upon the optical excitation level: a new weak peak appears first at the lower energy side of Peak 1, and rapidly emerges as a dominant spectral structure over Peak 1, as shown in Fig. 4. In addition to the extraordinary increase of its intensity, this new peak also significantly broadens and exhibits a noticeable red shift as the optical injection level is increased. In sharp contrast to the fascinatingly emerging peak, the peak position, line shape and linewidth of Peak 1 are all independent on the excitation level except for its intensity. The narrow linewidth and symmetric Lorentzian line shape suggest that Peak 1 is due to the fundamental band edge exciton emission. Moreover, its peak energy position, 2.017 eV, is close to the theoretical band gap of 2.1 eV for ideal WS_2 monolayers without considering the exciton effect.[17] Therefore, Peak 1 is ascribed to

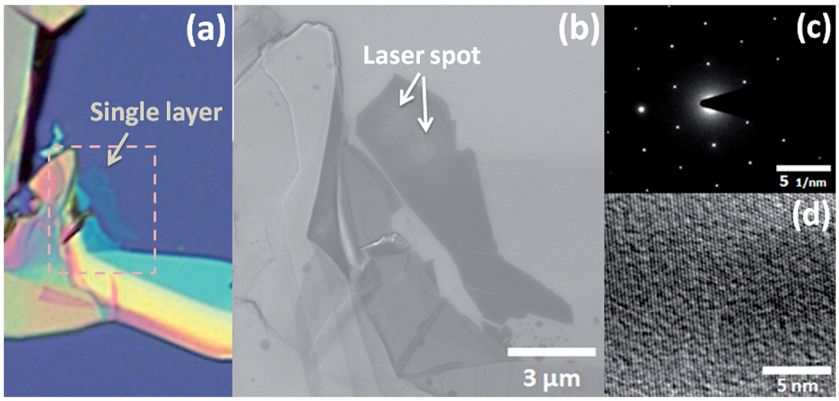

Fig. 1 (a) Optical and (b) SEM image of the exfoliated WS_2 sample. Single layers can be distinguished from multiple layers due to their distinctive contrast in the images. The laser exposure spots on the single layer are indicated by arrows in the SEM image. (c) Selected area electron diffraction patterns. (d) High-resolution transmission electron microscopic image of a monolayer WS_2 sample.

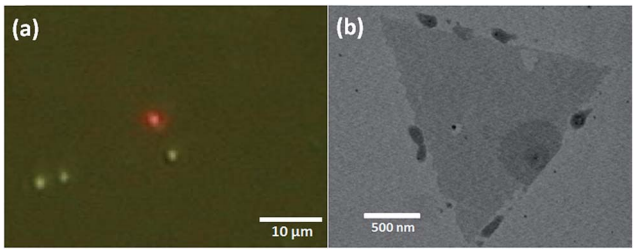

Fig. 2 (a) Optical and (b) SEM image of a furnace-grown triangle WS_2 monolayer. The red spot in (a) represents red color luminescence from a micro-scale region on the triangle WS_2 monolayer illuminated by a focused 514.5 nm laser beam.

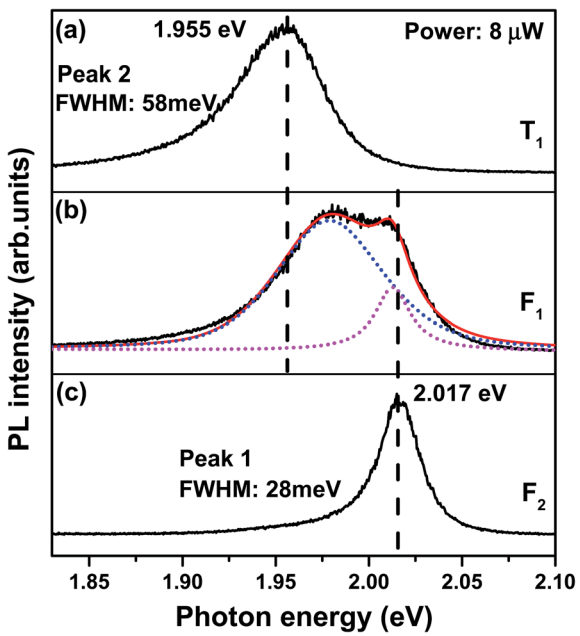

Fig. 3 Micro-PL spectra of the three monolayer WS_2 samples at room temperature under the conditions of weak excitation. Among them F_1 and F_2 are the two mechanically exfoliated samples while T_1 is a furnace-grown triangle sample.

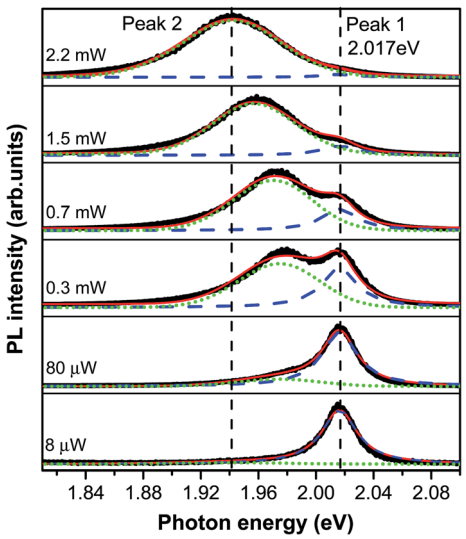

Fig. 4 Micro-PL spectra of sample F_2 at different optical excitation levels. Fascinatingly, the emission dominance of the sample can be tuned from Peak 1 to Peak 2. Peak 1 can be fitted well by a Lorentzian line shape function with a constant peak position and linewidth (dashed curves), while Peak 2 is fitted well by the LSE model (dotted curves). The peak positions of Peak 1 and 2 are marked in vertical dashed lines.

be the neutral band edge free exciton emission of a flawless WS_2 monolayer. If this assignment is correct, the binding energy of the free excitons in WS_2 monolayers could be ~83 meV provided that the theoretical fundamental bandgap of WS_2 monolayers is 2.10 eV.

Now we are in position to give more detailed arguments on Peak 2. First of all, the spin-orbit-split double valence bands shall be ruled out as the origin of this emission band due to an energy separation as large as 400 meV between the two spin-orbit-split bands.[16,18] Moreover, Peak 2 was located at the lower energy side of Peak 1. Secondly, trions, one kind of charged exciton having extra electrons or holes, are likely not to be the origin of Peak 2, at least not the main origin because

a trion emission peak is usually a weak structure near the neutral exciton peak, and has a smaller energy separation with the neutral free exciton emission.[19] In addition, Peak 2 quickly develops into a dominant spectral structure from an initial weak structure in sample F_2 as the optical excitation level increases. The photoinduced doping effect as demonstrated in graphene and related heterostructures[4,5] could be responsible for the appearance and eventual dominance of Peak 2. In the present study, Peak 2 in the furnace-grown triangle samples was almost independent of the excitation power regarding the peak position and linewidth, and in the exfoliated samples, the peak position and linewidth of Peak 2 displayed a strong dependence on the excitation level. Interestingly, all the three monolayer WS_2 samples show a great unified PL spectral feature at a high enough optical excitation level (*i.e.*, ≥2.0 mW). This unified spectral feature is that Peak 2 is dominant in the PL spectra of all the samples. In terms of the broad and asymmetric line shape of Peak 2, it could be localized state ensemble luminescence.

It is well known that there exist various mechanisms, *e.g.*, incorporating dopants and creating defects or disorders, leading to localized electronic states in semiconductors. For example, the theoretical study of Erementchouk *et al.* revealed that some vacancy defects may result in bound states within the band gap and relevant optical transitions on MoS_2 monolayers.[10] Kang *et al.* theoretically predicted that wave function localization could generally occur in many 2D TMD materials and heterostructures, and may have a strong impact on the electronic and optical properties of these ultimate materials.[20] If carriers occupy the localized states that have radiatively recombined, a broad emission band with an asymmetric line shape may be observed due to the wide energy distribution of localized states. For such a localized state ensemble (LSE) PL, a generalized model has been formulated as:[21]

$$\mathrm{PL}(E,T) \propto \rho(E) \times f(E,T) = \rho_0 \mathrm{e}^{-(E-E_0)^2/2\sigma^2} \times \frac{1}{\mathrm{e}^{(E-E_\mathrm{a})/k_\mathrm{B}T} + C}, \quad (1)$$

where $\rho(E)$ is a Gaussian-type density of states (DOS) of a defect state ensemble, $f(E,T)$ is a distribution function of carriers localized at some defects, E_0 is the central energy of DOS, E_a is somehow the Fermi level-like characteristic energy depending on the material, and ρ_0 and C are the two constants depending on the materials. As seen in Fig. 3, Peak 2 can be fitted very well with the LSE model described by eqn (1) with E_a values of 2.009 eV ± 2 meV.

We also examined the PL intensity dependence of Peak 1 and 2 of sample F_1 on the optical excitation level, as shown (full logarithmic scales) in Fig. 5. Evidently, Peak 2's intensity increases much faster than Peak 1's does so that an X-type crossing-over phenomenon was observed for the PL intensities of Peak 1 and 2. In fact, the sum of the integrated intensities of Peak 1 and Peak 2 follows a linear dependence on the excitation intensity when the excitation level is not very high, as seen in the inset in Fig. 5. The solid diamonds represent the total measured intensity of Peak 1 and Peak 2 while the solid line is a linear fitting to the experimental data. In general, the

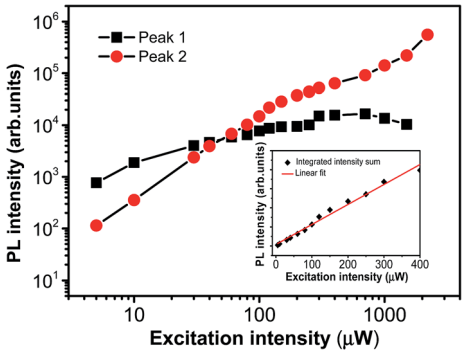

Fig. 5 Integrated PL intensity as a function of the laser power for Peak 1 and 2. Peak 2's intensity increases much faster so that an X-type crossing-over behavior appears for the PL intensities of Peak 1 and 2. The inset shows the total intensity of Peak 1 and Peak 2 *versus* the excitation intensity. The solid diamonds represent the experimental data while the solid line is a linear fit to the experimental data.

measured luminescence intensity, I_l, can be expressed in terms of the geometric collection factor, quantum efficiency, excitation light intensity *etc.* as:[22]

$$I_\mathrm{l} = C_\mathrm{g}\eta I_0(1 - 10^{-\mathrm{OD}}), \quad (2)$$

where C_g is the geometric collection factor which is a constant for a particular photoluminescence experimental setup, η is the quantum efficiency of luminescent transition, I_0 is the excitation light intensity, and OD is the optical density of the material which is proportional to the absorption coefficient. Obviously, the measured luminescence intensity is linearly dependent on the excitation light intensity according to eqn (2). As shown in the inset in Fig. 5, the measured total luminescence intensity of Peak 1 and Peak 2 indeed obeys the linear law. This indicates that the overall luminescence from the sample is still within the range of linear optics, despite the fact that Peak 2's intensity shows a super linear dependence on the excitation level.

We also note in Fig. 4 that a substantial red shift was observed for the peak position of Peak 2 with increased excitation intensity, whereas the peak position of Peak 1 basically remains unchanged. The heating effect can be ruled out as the physical origin causing the significant red shift of Peak 2 because Peak 1 did not shift. Band gap renormalization caused by the many-body effect could be the main mechanism of the observed substantial red shift of Peak 2. It is known that when the carrier population density becomes high enough due to optical excitation or impurity doping, the exchange and correlation effects among carriers become noticeable, which leads to the so-called renormalization effect. As a result of the renormalization effect, band gap shrinking takes place, and a red shift in the emission peak position could be observed.[23] An empirical formula for the band gap shrinking due the exchange and correlation interactions can be described as:[23] $\Delta E_\mathrm{B} \propto n^{1/3}$ and hence $\Delta {E_\mathrm{B}}^3 \propto n$, where n is the carrier density and it should be proportional to the excitation level or intensity. Indeed, the energy shift cube of Peak 2 shows a good linear dependence on the excitation level except for the data points under the conditions of extremely weak excitation.

Conclusions

To conclude, a photoinduced doping effect was demonstrated in exfoliated WS_2 monolayers at room temperature, mainly evidenced by the transition of light emission dominance from Peak 1 to Peak 2. Peak 1 is manifested as a narrow and symmetric peak of the free excitons, whereas Peak 2 is characterized by a broad and asymmetric peak of the localized electronic states. This photoinduced effect not only leads to a state-of-the-art understanding of the light emission nature of 2D WS_2 monolayers but also may have technological significance in the practical applications of these ultimate optoelectronic materials.

Acknowledgements

One of the authors, S.J.X., would like to acknowledge support from the University Development Fund and the SRT on New Materials of HKU, as well as HK-UGC AoE Grants (Project No.: AoE/P-03/08). We thank Dr K.Q. Hong for growing the furnace-grown samples. Dr H.L. Zeng was engaged in the initial PL measurements of the exfoliated samples and contributed valuable discussion. X.H.W. and S.J.X. wish to thank Prof. X.D. Cui for drawing our attention to trions.

References

1 Q. H. Wang, K. Kalantar-Zadeh, A. Kis, J. N. Coleman and M. S. Strano, *Nat. Nanotechnol.*, 2012, **7**, 699.
2 A. Splendiani, L. Sun, Y. Zhang, T. Li, J. Kim, C. Y. Chim, G. Galli and F. Wang, *Nano Lett.*, 2010, **10**, 1271.
3 K. F. Mak, C. Lee, J. Hone, J. Shan and T. F. Heinz, *Phys. Rev. Lett.*, 2010, **105**, 136805.
4 E. Alexeev, J. Moger and E. Hendry, *Appl. Phys. Lett.*, 2013, **103**, 151907.
5 L. Ju, J. Velasco Jr, E. Huang, S. Kahn, C. Nosiglia, H. Z. Tsai, W. Yang, T. Taniguchi, K. Watanabe and Y. Zhang, *Nat. Nanotechnol.*, 2014, **9**, 348.
6 N. Kang, H. P. Paudel, M. N. Leuenberger, L. Tetard and S. I. Khondaker, *J. Phys. Chem. C*, 2014, **118**, 21258.
7 X. H. Wang, J. Q. Ning, C. C. Zheng, B. R. Zhu, L. Xie, H. S. Wu and S. J. Xu, *J. Mater. Chem. C*, 2015, **3**, 2589.
8 P. K. Chow, R. B. Jacobs-Gedrim, J. Gao, T.-M. Lu, B. Yu, H. Terrones and N. Koratkar, *ACS Nano*, 2015, **9**, 1520.
9 J. H. Hong, Z. X. Hu, M. Probert, K. Li, D. H. Lv, X. N. Yang, L. Gu, N. N. Mao, Q. L. Feng, L. M. Xie, J. Zhang, D. Z. Wu, Z. Y. Zhang, C. H. Jin, W. Ji, X. X. Zhang, J. Yuan and Z. Zhang, *Nat. Commun.*, 2015, **6**, 6293.
10 M. Erementchouk, M. A. Khan and M. N. Leuenberger, *Phys. Rev. B: Condens. Matter Mater. Phys.*, 2015, **92**, 121401.
11 A. Pospischil, M. M. Furchi and T. Mueller, *Nat. Nanotechnol.*, 2014, **9**, 257.
12 B. W. H. Baugher, H. O. H. Churchill, Y. Yang and P. Jarillo-Herrero, *Nat. Nanotechnol.*, 2014, **9**, 262.
13 J. S. Ross, P. Klement, A. M. Jones, N. J. Ghimire, J. Yan, D. G. Mandrus, T. Taniguchi, K. Watanabe, K. Kitamura and Y. Wang, *Nat. Nanotechnol.*, 2014, **9**, 268.
14 K. F. Mak, K. L. McGill, J. Park and P. L. McEuen, *Science*, 2014, **344**, 1489.
15 H. R. Gutiérrez, N. Perea-López, A. L. Elías, A. Berkdemir, B. Wang, R. Lv, F. López-Urías, V. H. Crespi, H. Terrones and M. Terrones, *Nano Lett.*, 2012, **13**, 3447.
16 H. L. Zeng, G. B. Liu, J. F. Dai, Y. Yan, B. R. Zhu, R. C. He, L. Xie, S. J. Xu, X. H. Chen, Y. Wang and X. D. Cui, *Sci. Rep.*, 2013, **3**, 1608.
17 A. Kuc, N. Zibouche and T. Heine, *Phys. Rev. B: Condens. Matter Mater. Phys.*, 2011, **83**, 245213.
18 J. Kang, S. Tongay, J. Zhou, J. B. Li and J. Q. Wu, *Appl. Phys. Lett.*, 2013, **112**, 012111.
19 A. M. Jones, H. Yu, N. J. Ghimire, S. Wu, G. Aivazian, J. S. Ross, B. Zhao, J. Yan, D. G. Mandrus and D. Xiao, *Nat. Nanotechnol.*, 2013, **8**, 634.
20 J. Kang, J. B. Li, S.-S. Li, J.-B. Xia and L.-W. Wang, *Nano Lett.*, 2013, **13**, 5485.
21 Q. Li, S. J. Xu, M. H. Xie and S. Y. Tong, *Europhys. Lett.*, 2005, **71**, 994.
22 J. Garcia Sole, L. E. Bausa and D. Jaque, *An Introduction to the Optical Spectroscopy of Inorganic Solids*, John Wiley & Sons, Ltd, West Sussex, England, 2005, ch. 1, p. 20.
23 Y. J. Wang, S. J. Xu, Q. Li, D. G. Zhao and H. Yang, *Appl. Phys. Lett.*, 2006, **88**, 041903.